Compact antennas for digital TV reception on mobile terminals

R. Gaffoglio[1*], A. De Vita[2], B. Sacco[2], G. Giordanengo[1], M. Zucchi[3] and G. Vecchi[3].

[1] Advanced Computing and Applications, Fondazione LINKS, Torino, Italy
[2] Centre for Research, Technology Innovation and Experimentation, RAI Radiotelevisione Italiana, Torino, Italy
[3] Department of Electronics and Telecommunications, Politecnico di Torino, Torino, Italy
[*] Corresponding author: rossella.gaffoglio@linksfoundation.com

Abstract: The possibility to design compact broadband antennas for digital television reception on mobile terminals conflicts with the physical constraints imposed by the small size of the devices. To the best of our knowledge, the only attempt reported in literature refers to the excitation of the mobile device's metal structure (*chassis*) by means of coupling elements (CE), moving its resonances across the whole digital terrestrial television (DTT) band with a matching circuit. Starting from the examples reported in literature, we simulated the behavior of the CE-based antennas in COMSOL Multiphysics® for different device sizes, and different positions of the coupling element. The simulated results have been compared to the experimental data obtained from the implementation of three different prototypes, showing a good agreement between simulations and measurements.

Keywords: broadband antennas, digital terrestrial television (DTT), digital video broadcasting (DVB), directivity, genetic algorithm, mobile terminals, planar inverted-F antenna (PIFA).

1. Introduction

With Release 14, the Third Generation Partnership Project (3GPP) [1] paved the way to the possibility of delivering digital television services on mobile terminals, such as smartphones and tablets, overcoming all the limitations of the previous releases. From the receiver's point of view, this poses a great challenge for the antenna designers, due to the wide band to cover with a sufficient return loss, i.e., the whole digital terrestrial television (DTT) band (470-694 MHz), and the limited volume available for the antennas on a mobile device. To deal with the limits on the achievable bandwidth characterizing the performance of small antennas, the only solution seems to be the possibility to excite the characteristic modes of the ground layers and metal shielding of the entire device (i.e., the so-called *chassis*) by means of properly-shaped coupling structures [2,3]. In addition to the configurations proposed by Holopainen et al. [2], with the coupling element (CE) placed on the short edge of the chassis, we analyzed the excitation of a higher characteristic mode of the chassis via a CE located on the long edge [4].
Three prototypes have been experimentally realized: a smartphone-type chassis with dimensions 135 mm x 75 mm x 5 mm, with the CE placed on the short edge, a bigger smartphone-type model with dimensions 160 mm x 90 mm x 5 mm and the CE positioned on the longer edge, and a tablet-size model with dimensions 200 mm x 130 mm x 7 mm with the CE on the long edge. The CE structure simply consists in a folded metal sheet forming a sort of stair step with fixed height. All the prototypes have been modeled in COMSOL Multiphysics® using the RF module and reproducing the experimental feeding near the CE element by means of a coaxial cable excited by a Lumped Coaxial Port. For these antennas, the reliability of the S11 curve is crucial, since it is used to evaluate the matching circuit elements needed to properly shift the resonant behavior across the DTT band.
This paper reports the description of the CE-based antennas and the COMSOL model reproducing the antenna prototypes in Sections 2 and 3, respectively. The implemented models allowed us to study the behavior of the S11 curves for the different configurations, and to evaluate the matching components needed to move the resonance towards the DTT band in order to ensure a sufficiently low return loss across the whole band. The experimental realization of the prototypes, the acquired measurements and the comparison with the simulation results are reported in Section 4.
Finally, the performance of the considered CE-based antennas has been compared to that of a planar inverted F-antenna (PIFA), optimized to show a self-resonant behavior across the DTT band by means of a genetic algorithm implemented in COMSOL Multiphysics using the LiveLink™ for MATLAB® module (Section 5). The conclusions follow in Section 6.

2. CCE-based antenna solutions

The effect of the conducting mobile terminal chassis on an embedded low-volume antenna structure (like a PIFA) has been examined in literature [5]. The results show that, especially at the lower frequencies

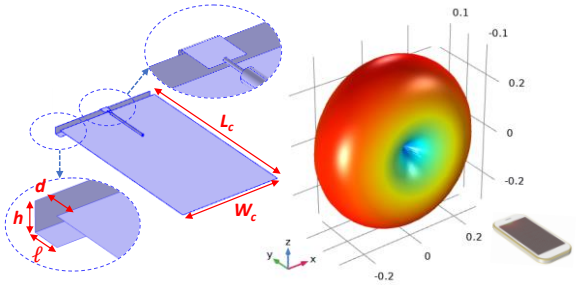

Figure 1. Coupling element-based antenna with the CE on the short edge (SE) (*left*) with the respective Far-field norm pattern computed with COMSOL Multiphysics (*right*).

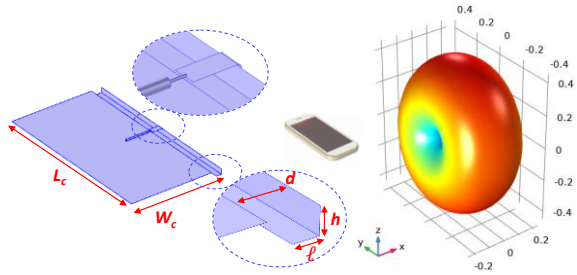

Figure 2. Coupling element-based antenna with the CE on the long edge (LE) (*left*) with the respective Far-field norm pattern computed with COMSOL Multiphysics (*right*).

of operation (below 900 MHz), the chassis is almost the only radiating part, while the antenna element acts as a coupler between the antenna feed and the chassis [5], [6]. Hence, the main part of the power is radiated by the half-wave dipole-type current distribution of the chassis, which corresponds to its first resonant mode. These considerations suggest that the bandwidth of an antenna-chassis combination can be improved by enhancing the coupling from the antenna element to the dominating characteristic wavemode of the chassis. This can be done by means of a non-resonant Capacitive Coupling Element (CCE), i.e., a properly placed folded metal sheet able to efficiently excite the characteristic modes of the chassis. To maximize the coupling, it was demonstrated that the CCE needs to be placed at the ends of the ground plane, totally outside the chassis [5].

In addition to the antenna configuration with the CCE located on the chassis short edge (SE) [2] (which basically excites the chassis fundamental characteristic mode), we analysed the excitation of the second characteristic mode by moving the CCE on the long edge (LE) (see Figs. 1 and 2 for the layouts considered in our study).

3. COMSOL model

To analyze the CCE-type antennas from a simulative point of view, we reproduced the antenna-chassis structures in COMSOL Multiphysics, as reported in

Table 1. Geometrical dimensions of the implemented prototypes expressed in mm.

Prot. #	CCE	L_C	W_C	h	d	ℓ
1	SE	135	75	5	5	5
2	LE	160	90	5	10	5
3	LE	200	130	7	10	5

Figs. 1 and 2. The chassis is simply modeled as an infinitely thin PEC layer with dimensions $W_c \times L_c$. The CCE is placed at a distance d from the chassis, and is modeled as a folded PEC sheet with zero thickness, length ℓ and height h. The coupling element is connected to the inner wire of a coaxial cable by means of a metal tab modeled to accurately reproduce the connection between the CCE and the chassis realized in the laboratory on the prototypes (see the insets of Figs. 3,4). The coaxial cable was properly sized to ensure a characteristic impedance of 50 Ω and was fed with a Coaxial Lumped Port applied at its end.

Finally, a Polystyrene block ($\varepsilon_r = 2.3, \tan\delta = 0.0002$) with dimensions $W_c \times d \times h$ for the SE model and $d \times L_c \times h$ for the LE case was inserted between the chassis and the CCE element to reproduce the support added in the experimental prototypes in order to increase their robustness.

The antenna models were placed in a spherical air domain, surrounded by a spherical PML layer, and the far-field domain calculation feature was introduced to determine the electromagnetic field distribution at great distances from the antennas.

4. Results

The geometrical characteristics of the prototypes experimentally realized are summarized in Table 1. As can be seen in the insets of Figs. 3,4, the inner

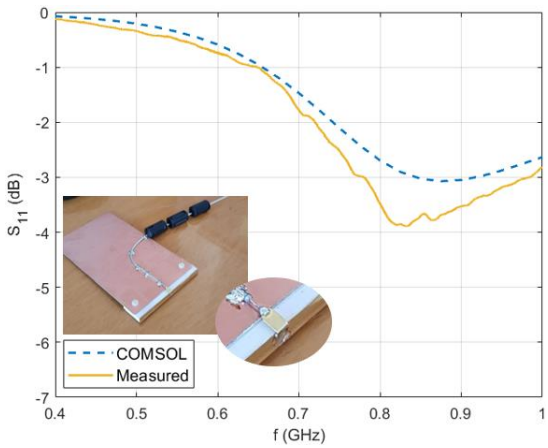

Figure 3. Reflection coefficient evaluated near the coupling element for the simulated and implemented prototype #1 (see Table 1).

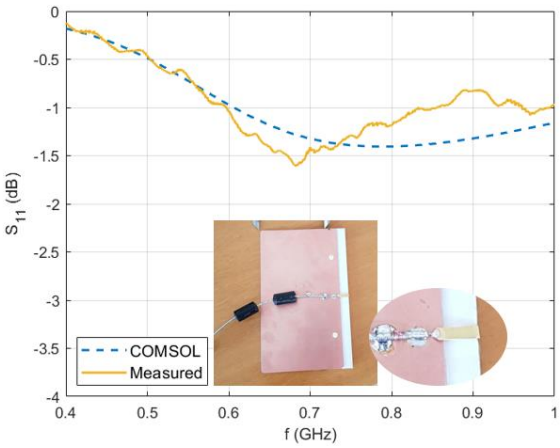

Figure 4. Reflection coefficient evaluated near the coupling element for the simulated and implemented prototype #2 (see Table 1).

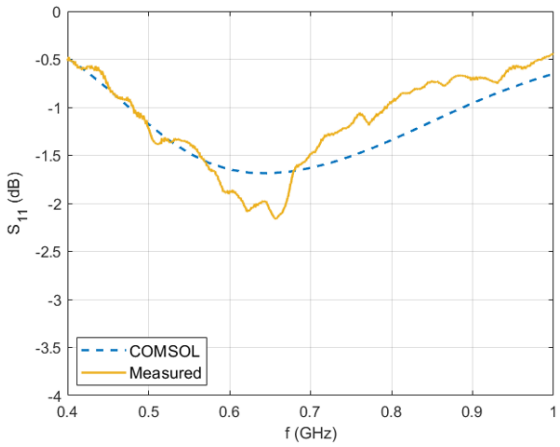

Figure 5. Reflection coefficient evaluated near the coupling element for the simulated and implemented prototype #3 (see Table 1).

wire of the coaxial cable has been welded to a tab connected to the coupling element, while its outer layer was soldered in different points on the metal ground forming the chassis. A series of ferrite chokes was added around the cable to minimize interference and ensure signal integrity.

4.1 Reflection coefficient

COMSOL Multiphysics allowed us to directly compute the reflection coefficient (S11 parameter) on the coaxial port at different simulation frequencies in the range 0.4 GHz - 1 GHz; it was then possible to compare the simulated results to those obtained performing a dense frequency sweep on the prototypes with a Vector Network Analyzer (VNA). A sufficiently good agreement between the numerical and experimental results (Figs. 3-5) is observed for all the considered prototypes.

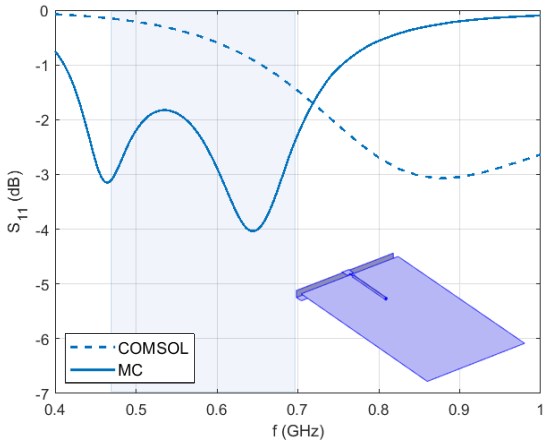

Figure 6. Reflection coefficient for the prototype #1 before (dashed line) and after (solid line) the introduction of a suitable matching circuit.

From all the reported S11 curves it appears evident that the considered structures resonate outside the DTT band, at a frequency which increases when the antenna dimensions are smaller. However, these simple antennas can be matched across the DTT band by introducing a proper matching circuit [2]. Fig. 6 shows how the S11 curve obtained with COMSOL for the prototype #1 (Fig. 3) can be matched across the DTT band by introducing a multi-resonant optimized circuit made of 2 inductors and 1 capacitor. Although the return loss still seems very high in the DTT band (blue region), it is lower than -1.5 dB, which is the upper threshold considered in [2] for the return loss according to the DVB-H specifications [7]. We have verified that the matching procedure carried out on the experimental S11 curve leads to a matching circuit which is very similar to that found using the simulated curve (the differences on the matching elements were found on the order of 2-3 nH for the inductors and 1 pF for the capacitor).
The robustness of the numerical results allows to perform *a priori* optimization of the chassis-CCE structure, providing a realistic forecast of what will be the coverage quality in the DTT band.

4.2 Radiation pattern

The Far-field calculation feature in COMSOL Multiphysics allowed us to analyze the radiation pattern of the simulated antenna solutions. To derive the polar plot of the directivity from the Gain function directly provided by COMSOL, we first evaluated the total radiated power by computing the surface integral of the time-averaged power outflow (normal Poynting vector) on the spherical surface surrounding the computational domain:

$$P_{rad} = \int_0^{\pi} \int_0^{2\pi} \text{emw.nPoav } d\Omega, \qquad (1)$$

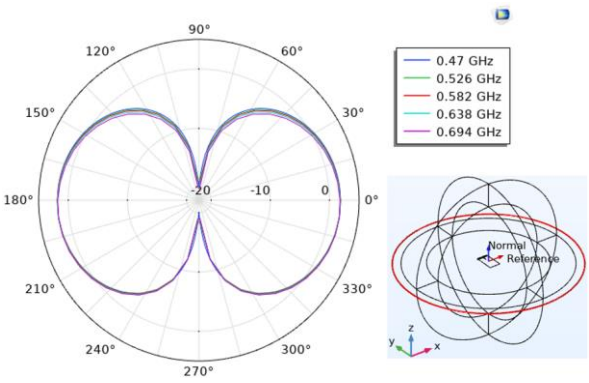

Figure 7. Directivity patterns on the *xy* plane relative to the prototype #1 at different frequencies, evaluated with COMSOL Multiphysics.

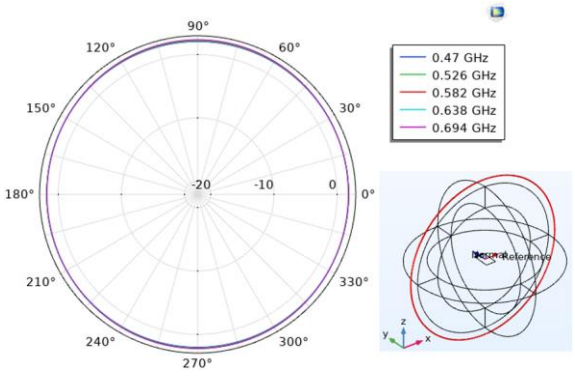

Figure 8. Directivity patterns on the *xz* plane relative to the prototype #1 at different frequencies, evaluated with COMSOL Multiphysics.

being $d\Omega$ the solid angle. The incident power P_{in} can be written as: $|V_0|^2/2Z_0$, where $V_0 = 1$ V is the applied voltage, while $Z_0 = 50\,\Omega$ is the characteristic impedance of the coaxial lumped port. From the definition of the antenna total efficiency:

$$\eta_{tot} = \eta_{rad}(1 - |S_{11}(f)|^2) = \frac{P_{rad}}{P_{in}} \qquad (2)$$

the radiation efficiency $\eta_{rad}(f)$ can be derived for the different frequencies.
This allows to evaluate the directivity from the antenna gain using the following expression:

$$D(\theta, \phi, f) = \frac{G_{COMSOL}(\theta, \phi, f)}{\eta_{rad}(f)}. \qquad (3)$$

The directivity for the prototype #1 is reported in Figs. 7 and 8 on the *xy* and *xz* plane, respectively, for 5 evenly spaced frequencies in the DTT range.
The simulated results are compared to the experimental measurements performed on the prototype #1 with a compact bench-top electromagnetic scanner (EM-Scan RFX [8]) that allows a real time antenna characterization in the laboratory environment. Figs. 9 and 10 show the

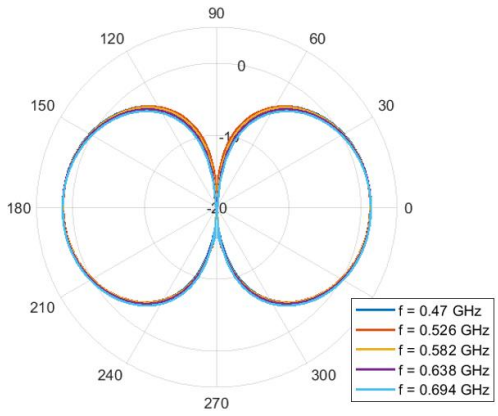

Figure 9. Directivity patterns on the *xy* plane relative to the prototype #1 at different frequencies, experimentally evaluated with the EM-Scan RFX.

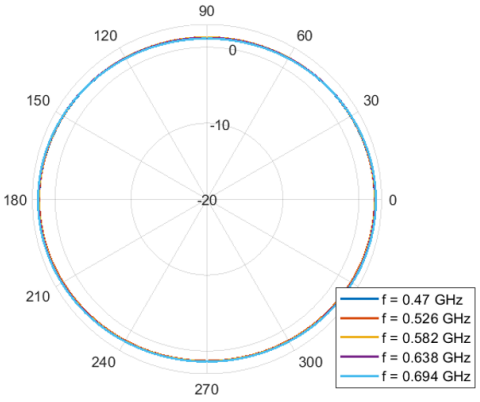

Figure 10. Directivity patterns on the *xz* plane relative to the prototype #1 at different frequencies, experimentally evaluated with the EM-Scan RFX.

directivity patterns evaluated with the EM scanner on the *xy* and *xz* plane, respectively, for the selected 5 frequency samples in the DTT range. By comparing Fig. 7 to Fig. 9 and Fig. 8 to Fig. 10, a good agreement between the measured and simulated results can be observed at all the considered different frequencies.

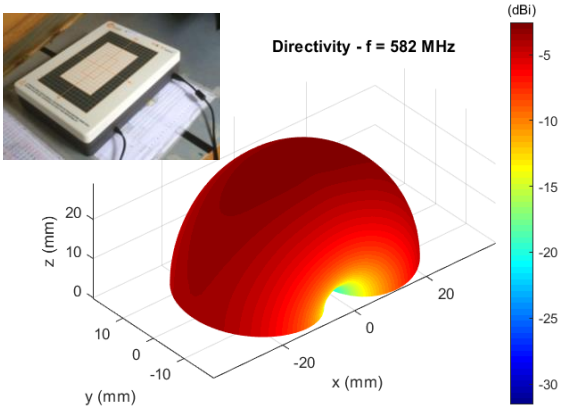

Figure 11. Directivity pattern computed by the EM-Scan (inset) at f = 582 MHz for the prototype #1.

Table 2. Radiation efficiency and maximum directivity for the antenna prototype #1.

f (MHz)	η_{rad} (COMSOL)	D_{max} (dBi) (COMSOL)	D_{max} (dBi) (EM-Scan)
470	0.8969	1.96	2.23
526	0.9382	2.02	2.19
582	0.9586	2.10	2.21
638	0.9691	2.19	2.23
694	0.9747	2.29	2.29

The satisfactory agreement is also confirmed by Table 2, which reports a comparison at the different frequencies between the maximum directivity values computed with COMSOL and those measured with the EM scanner.
Finally, for completeness, Fig. 11 reports the tridimensional directivity pattern evaluated with the EM-Scan at f = 582 MHz for the prototype #1.

5. PIFA optimization

In this last section, we report our attempts to increase the bandwidth of a self-resonant antenna solution, creating non-intuitive sequences of slots in the metal coverage of the antenna by means of a genetic algorithm. The considered self-resonant structure is a Planar Inverted-F Antenna (PIFA), which is a very popular solution in mobile communications, being low profile, conformal, easy to design, low cost and reliable [9]. This antenna consists of a ground plane, a radiating patch above the ground plane, a feeding pin, and a shorted sheet.

5.1 Genetic Algorithms

A Genetic Algorithm (GA) consists of a population of candidate solutions (called *individuals*) for an optimization problem evolving toward better solutions. Each candidate solution has a set of properties (its *chromosomes*), usually coded in a string of bits, which can be mutated and altered [10]. The evolution starts from a population of randomly generated individuals, and it is an iterative process, with the population in each iteration called *generation*. The "quality" of each individual is estimated by means of a *fitness function*, which is usually the objective function in the optimization problem being solved. At each iteration, a selection is performed on the individuals in order to decide which are more likely to reproduce based on their fitness. The reproduction takes place by means of the so-called *crossover* (or recombination), which is a genetic operator used to combine the genetic information of two parents to generate new offspring. This generational process is repeated until

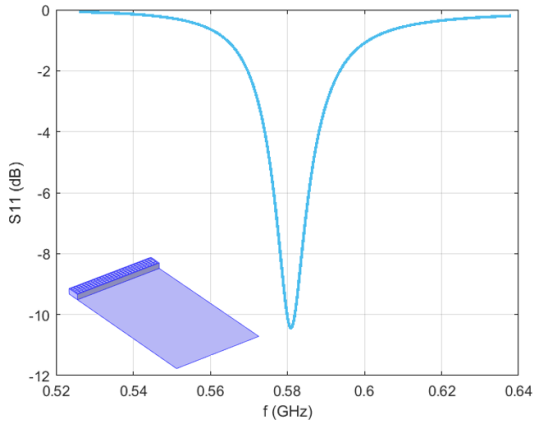

Figure 12. Narrowband behavior of the PIFA, designed to resonate at f = 582 MHz.

a termination condition or a fixed number of generations has been reached.
The application of the GA to the optimization of the PIFA can be described as follows. First, the dimensions of the PIFA were optimized to make the antenna resonate at f = 582 MHz (see Fig. 12), according to the PIFA design equations [9]. Then, the metal coverage of the antenna was divided into an arbitrary number N_g of small sectors (*number of genes* of each individual). Each independent portion is represented by a bit in the chromosome: 1 means the presence of metal, while 0 means that it is removed. Hence, each sequence of N_g bits represents a single individual, which corresponds to a particular metal configuration for the considered antenna. Fig. 13 shows the PIFA simulated with COMSOL Multiphysics, where the metal patch and the corresponding portion on the ground plane have been subdivided into N_g = 532 sectors. For each individual, the following fitness function was estimated:

$$F = \frac{1}{N_f}\sum_{i=1}^{N_f} Q(f_i), \tag{4}$$

with:

$$Q(f_i) = \begin{cases} S_{11}(f_i) & \text{if } S_{11}(f_i) \geq th \\ th & \text{if } S_{11}(f_i) < th \end{cases} \tag{5}$$

where N_f is the total number of considered frequencies, $S_{11}(f_i)$ is the reflection coefficient in dB relative to the ith frequency, while *th* is a fixed threshold on the reflection coefficient. F represents the mean performance over the bandwidth in terms of reflection coefficient, while the threshold *th* was introduced in order to avoid the algorithm to converge towards single narrow-band well-matched solutions. Indeed, our objective was to obtain a configuration showing a reflection coefficient at least lower than -1.5 dB over the whole DTT band.

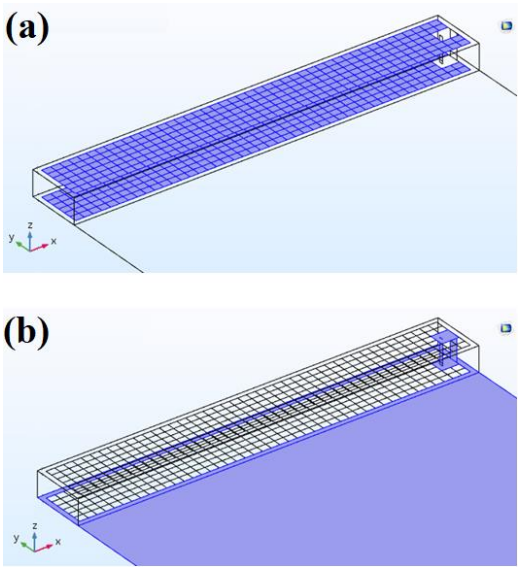

Figure 13. (a) Metal portion of the PIFA subdivided in 532 optimizable sectors; (b) metal regions that are not changed by the GA.

5.2 GA/COMSOL optimization

The optimization with the GA was performed by means of an iterative loop between MATLAB and COMSOL Multiphysics, using the LiveLink™ for MATLAB® module. For each design possibility dictated by the GA, COMSOL evaluates the corresponding fitness and returns this value to MATLAB. Fig. 14 shows the structure obtained running the genetic algorithm for 155 generations, a population composed by 200 individuals, th = -5 dB, and f = [526, 582, 638] MHz, with the purpose of inducing a multi-resonant behavior in the DTT band. Unfortunately, the implemented optimization has not provided any significant improvement. The mean S11 defined in (4) decreased by a very small amount, i.e., from -1.71 dB relative to the unchanged configuration to -1.77 dB for the configuration reported in the lower picture of Fig. 14, and the final S11 curve maintains a narrowband behavior similar to that of the starting configuration (Fig. 12).
The achieved results demonstrate how the PIFA cannot be a solution for the considered problem, neither as a self-resonant element (due to the limited dimensions dictated by the geometry of the device) nor as an exciting structure, confirming that the PIFA is not optimal to couple currents to the surface of the chassis [6].

6. Conclusions

The purpose to realize a compact wideband antenna able to cover the whole DTT band with a sufficient

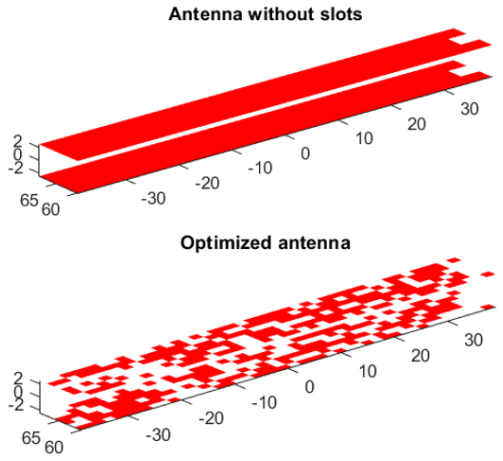

Figure 14. *Upper row*: PIFA fully covered by metal (no slot is present); *lower row*: slot configuration for the PIFA corresponding to the best (in terms of fitness) individual of the last generation.

return loss is very ambitious from a physical point of view, due to the limited volume available on a mobile device for the antenna element. The only way found in literature is represented by the attempt to exploit the whole planar dimension of the device, improving the excitations of the chassis characteristic modes by means of low-volume coupling structures.
In this paper, we analyzed this possibility with simulations performed in COMSOL Multiphysics, and the realization of three different prototypes. In addition to the configuration with the coupling element placed on the short edge of the chassis, we also investigated the possibility of exciting the second characteristic mode of the chassis by placing the CE on the long edge.
The good agreement between simulations and measurements suggests how COMSOL can be used to study and optimize the geometry of the CCE element in order to maximize the excitation of the chassis eigen-currents, with the aim of improving the matching in the DTT band after the introduction of a matching circuit.

7. References

[1] *3rd Generation Partnership Project (3GPP); technical specification group radio access network; study on scenarios and requirements for next generation access technologies*, (*Release 14*), 3GPP TR 38.913 V0.4.0, 2016.
[2] J. Holopainen, O. Kivekäs, C. Icheln, and P. Vainikainen, “Internal Broadband Antennas for Digital Television Receiver in Mobile Terminals”, *IEEE Trans. Antennas Propag.*, vol. 58, no. 10, pp. 3363-74, 2010.

[3] P. Vainikainen, J. Holopainen, and M. Kyrö, “Antennas for digital television receivers in mobile terminals”, *Proc. of the IEEE*, vol. 100, no. 7, pp. 2341-48, 2012.
[4] R. Gaffoglio, M. Zucchi, G. Vecchi, and B. Sacco, “A Numerical Analysis of Compact/ Wideband Antenna Performance for DTT Reception on Mobile Terminals”, *13th European Conference on Antennas and Propagation* (*EuCAP*), 2019.
[5] P. Vainikainen, J. Ollikainen, O. Kivekäs, and I. Kelander, “Resonator-based analysis of the combination of mobile handset antenna and chassis”, *IEEE Trans. Antennas Propag*., vol. 50, no. 10, pp. 1433-44, 2002.
[6] J. Villanen, J. Ollikainen, O. Kivekäs, and P. Vainikainen, “Coupling element based mobile terminal antenna structures”, *IEEE Trans. Antennas Propag*., vol. 54, no. 7, pp. 2142-53, 2006.
[7] *Digital Video Broadcasting (DVB); DVB-H Implementation Guidelines*, ETSI TR 102 377, version 1.4.1, 2009.
[8] *EM-Scan-RFX2-Datasheet*, Calgary, Canada.
[9] C. A. Balanis, *Antenna Theory: Analysis and Design*, 4th ed., John Wiley & Sons, 2016.
[10] D. S. Weile and E. Michielssen, “Genetic algorithm optimization applied to electromagnetics: a review,” *IEEE Trans. Antennas Propag*., vol. 45, no. 3, pp. 343-53, 1997.

8. Acknowledgments

We would like to thank the whole COMSOL technical support staff in Brescia for their availability and help.